

All-optical sampling and magnification based on XPM-induced focusing

J. NUÑO,¹ M. GILLES,¹ M. GUASONI,² C. FINOT,¹ AND J. FATOME^{1,*}

¹Laboratoire Interdisciplinaire Carnot de Bourgogne (ICB), UMR 6303 CNRS-Univ. Bourgogne Franche-Comté, 9 av. A. Savary, 21078 Dijon, France

²Nonlinear Physics Center, Australian National University, Canberra ACT 0200, Australia
*jfatome@u-bourgogne.fr

Abstract: We theoretically and experimentally investigate the design of an all-optical magnification and sampling function free from any active gain medium or additional amplified spontaneous noise emission. The proposed technique is based on the co-propagation of an arbitrary shaped signal together with an orthogonally polarized intense fast sinusoidal beating within a normally dispersive optical fiber. This process allows us to experimentally demonstrate a 40-GHz sampling operation as well as an 8-dB magnification of an arbitrary shaped nanosecond signal around 1550 nm in a 5-km long optical fiber. The experimental observations are in good agreement with numerical and theoretical analysis.

© 2016 Optical Society of America

OCIS codes: (060.4370) Nonlinear optics, fibers; (070.4340) Nonlinear optical signal processing; (190.4380) Nonlinear optics, four-wave mixing.

References and links

1. M. A. Duguay and J. W. Hansen, "An ultrafast light gate," *Appl. Phys. Lett.* **15**(6), 192–194 (1969).
2. T. Kanada and D. L. Franzen, "Optical waveform measurement by optical sampling with a mode-locked laser diode," *Opt. Lett.* **11**(1), 4–6 (1986).
3. H. Ohta, S. Nogiwa, N. Oda, and H. Chiba, "Highly sensitive optical sampling system using timing-jitter-reduced gain-switched optical pulse," *Electron. Lett.* **33**(25), 2142–2144 (1997).
4. I. Shake, E. Otani, H. Takara, K. Uchiyama, Y. Yamabayashi, and T. Morioka, "Bit rate flexible quality monitoring of 10 to 160 Gb/s optical signals based on optical sampling technique," *Electron. Lett.* **36**(25), 2087–2088 (2000).
5. R. L. Jungerman, G. Lee, O. Buccafusca, Y. Kaneko, N. Itagaki, R. Shioda, A. Harada, Y. Nihei, and G. Sucha, "1-THz bandwidth C- and L-Band optical sampling with a bit rate agile timebase," *IEEE Photonics Technol. Lett.* **14**(8), 1148–1150 (2002).
6. T. Suhara, H. Ishizuki, M. Fujimura, and H. Nishihara, "Waveguide quasi-phase-matched sum-frequency generation device for high-efficiency optical sampling," *IEEE Photonics Technol. Lett.* **11**(8), 1027–1029 (1999).
7. S. Nogiwa, Y. Kawaguchi, H. Ohta, and Y. Endo, "Highly sensitive and time-resolving optical sampling system using thin PPLN crystal," *Electron. Lett.* **36**(20), 1727–1728 (2000).
8. N. Yamada, S. Nogiwa, and H. Ohta, "640 Gb/s OTDM signal measurement with high-resolution optical sampling system using wavelength-tunable soliton pulses," *IEEE Photonics Technol. Lett.* **16**(4), 1125–1127 (2004).
9. J. Li, J. Hansryd, P. O. Hedekvist, P. A. Andrekson, and S. N. Knudsen, "300-Gb/s eye-diagram measurement by optical sampling using fiber-based parametric amplification," *IEEE Photonics Technol. Lett.* **13**(9), 987–989 (2001).
10. S. I. Oda, A. Maruta, and K. Kitayama, "All-optical quantization scheme based on fiber nonlinearity," *IEEE Photonics Technol. Lett.* **16**(2), 587–589 (2004).
11. J. Li, M. Westlund, H. Sunnerud, B. E. Olsson, M. Karlsson, and P. A. Andrekson, "0.5-Tb/s eye-diagram measurement by optical sampling using XPM-induced wavelength shifting in highly nonlinear fiber," *IEEE Photonics Technol. Lett.* **16**(2), 566–568 (2004).
12. P. A. Andrekson and M. Westlund, "Nonlinear optical fiber based high resolution all-optical waveform sampling," *Laser Photonics Rev.* **1**(3), 231–248 (2007).
13. S. Zhang, Y. Liu, Y. Liu, and H. J. S. Dorren, "All-optical sampling exploiting nonlinear polarization rotation in a single semiconductor optical amplifier," *Opt. Commun.* **285**(6), 1001–1004 (2012).
14. C. Xu and X. Liu, "Photonic analog-to-digital converter using soliton self-frequency shift and interleaving spectral filters," *Opt. Lett.* **28**(12), 986–988 (2003).
15. R. Maram, J. Van Howe, M. Li, and J. Azana, "Noiseless intensity amplification of repetitive signals by coherent addition using the temporal Talbot effect," *Nat. Commun.* **5**, 5163 (2014).

16. J. Nuño, M. Gilles, M. Guasoni, B. Kibler, C. Finot, and J. Fatome, "40 GHz pulse source based on cross-phase modulation-induced focusing in normally dispersive optical fibers," *Opt. Lett.* **41**(6), 1110–1113 (2016).
17. T. Inoue and S. Namiki, "Pulse compression techniques using highly nonlinear fibers," *Laser Photonics Rev.* **2**(1–2), 83–99 (2008).
18. K. E. Webb, M. Erkintalo, Y. Q. Xu, G. Genty, and S. G. Murdoch, "Efficiency of dispersive wave generation from a dual-frequency beat signal," *Opt. Lett.* **39**(20), 5850–5853 (2014).
19. C. Fortier, B. Kibler, J. Fatome, C. Finot, S. Pitois, and G. Millot, "All-fibered high-quality low duty-cycle 160-GHz femtosecond pulse source," *Laser Phys. Lett.* **5**(11), 817–820 (2008).
20. Q. Z. Wang, P. P. Ho, and R. R. Alfano, "Degenerate cross-phase modulation for pulse compression and amplification of ultrashort laser pulses," *Opt. Lett.* **15**(18), 1023–1025 (1990).
21. J. Fatome, C. Finot, G. Millot, A. Armaroli, and S. Trillo, "Observation of Optical Undular Bores in Multiple Four-Wave Mixing," *Phys. Rev. X* **4**(2), 021022 (2014).
22. P. K. A. Wai, C. R. Menyuk, and H. H. Chen, "Stability of solitons in randomly varying birefringent fibers," *Opt. Lett.* **16**(16), 1231–1233 (1991).
23. G. P. Agrawal, *Nonlinear Fiber Optics*, 5th ed. (Academic Press, 2013).
24. E. Lichtman, R. G. Waarts, and A. A. Friesem, "Stimulated Brillouin scattering excited by a modulated pump wave in single-mode fibers," *J. Lightwave Technol.* **7**(1), 171–174 (1989).

1. Introduction

In modern photonic systems, the sampling process has widespread applications in the fields of optical communications, metrology, clocking, sensing, spectral comb or arbitrary waveform generation. In this context, nonlinear effects have been demonstrated as potential key technologies to develop all-optical sampling devices [1–14]. In most of these techniques, an ultrashort pulse train acts as an optical gate and the basic physical phenomena under use include four-wave mixing (FWM) [10], cross-phase modulation (XPM) [11], nonlinear polarization rotation [13] or Raman soliton self-frequency shifting [14]. On the other hand, signal amplification is also a critical function in many area of physics. Basically, optical amplification process refers to multiply an incident signal by increasing its global energy through an active gain medium pumped by an external pump beam. The large range of current and mature amplification techniques at telecommunication wavelengths involves Erbium doped fiber amplifiers, Raman-based amplifiers, semiconductor amplifiers or parametric processes. However, it is noteworthy that most of these techniques lead to an inherent degradation of the signal-to-noise ratio induced by the detrimental spontaneous emission of photons. More recently, Azaña and associates have suggested and experimentally validated a different scenario in which a linear redistribution of energy into a periodic pulse train through the self-imaging Talbot effect can lead to a noiseless amplification process [15].

In this manuscript, we propose an alternative nonlinear approach enabling to simultaneously sample and magnify an arbitrary shaped incident signal due to a focusing effect occurring in a normally dispersive medium through the cross-phase modulation induced by an orthogonally polarized high-repetition-rate sinusoidal sampling beam. Fundamentally, the strong sinusoidal beating is responsible for a localized and periodic focusing of the signal energy into high repetition pulses generated at the sampling modulation frequency [16]. This internal redistribution of energy within the signal wave leads to the generation of a temporal intensity comb whose amplitude is then directly proportional to the signal profile, thus inducing a simultaneous sampling and magnifying process. Based on this technique, we have experimentally demonstrated a 40-GHz sampling operation as well as an 8-dB magnification factor of an arbitrary shaped nanosecond signal around 1550 nm in a 5-km long normally dispersive fiber. We have also derived a theoretical estimation of the total magnifying factor of the system in good agreement with our experimental observations and numerical simulations based on a simplified Manakov modelling.

2. Principle and modeling of the sampling and magnification process

Basically, it is well-known that the anomalous dispersive regime of propagation in optical fibers can lead to a focusing effect owing to the interplay between chromatic dispersion and Kerr nonlinearity. This process has been exploited in numerous studies in order for instance

to compress optical pulses or design high-repetition pulse sources [17–19]. More recently, we have reported the observation of a focusing effect occurring in the normal dispersion regime through a XPM interaction between a weak periodic signal and its orthogonally polarized interleaved high-power replica [16]. In this previous configuration, a 3.3-ps 40-GHz pulse train was then generated [16]. In this new contribution, we exploit a similar physical mechanism [20] to induce a temporal focusing of an arbitrary shaped signal so as to sample and magnify its intensity profile. As a rule of thumb, the signal to be processed is co-propagating in a normally dispersive optical fiber of length L together with a sinusoidal sampling beam. In the present configuration, the sampling wave (that we also may call the pump even if no energy transfer occurs) consists in a much more intense orthogonally polarized high-repetition-rate carrier-suppressed beat-signal. As depicted in Fig. 1(a), due to the nonlinear defocusing dynamics of the fiber, the sampling beam is reshaped into parabolic then into broad and sharp square pulses. Subsequently, optical shocks associated to wave-breaking phenomenon appear in its intensity profile inducing undular bores that are nucleated from the breaking points at nulls and expand outwards [21]. As these singularities propagate, they are characterized by steeper and steeper edges, and then progressively collapse. In parallel, the XPM nonlinear phase shift induced by these nonlinear dark structures combined with the group velocity dispersion of the fiber then turns out the normal dispersion regime into a periodic focusing dynamics for the co-propagating signal. Consequently, as shown in Fig. 1(b), a fast and periodic pulse train exactly proportional to the incident signal is then generated, thus inducing a discrete sampling and an overall magnification effect of its intensity profile.

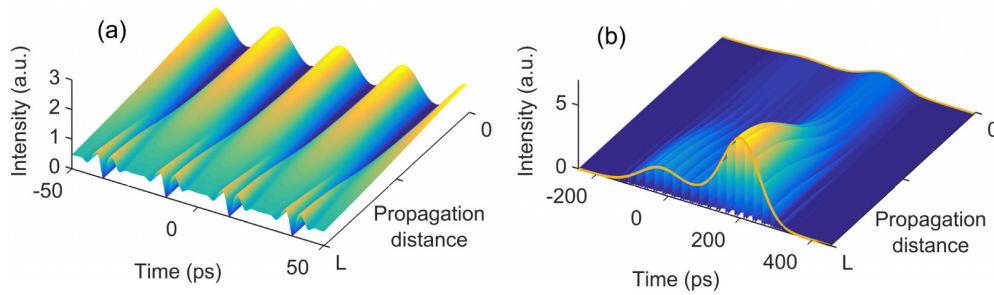


Fig. 1. Longitudinal evolution of the temporal intensity profiles of the sampling and signal waves (panels (a) and (b), respectively). L is for fiber length.

Figures 2(a) and 2(c) show a numerical illustration of this process. For these simulations, we consider two orthogonally polarized optical waves propagating in a normally dispersive randomly birefringent fiber. The evolution of the complex slowly varying amplitudes of the signal u and sampling wave v are described by the following set of two coupled nonlinear Schrödinger equations, corresponding to a simplified Manakov model [22] in which nonlinear terms involved with the weaker signal have been neglected:

$$\begin{cases} i \frac{\partial u}{\partial z} - \frac{\beta_2}{2} \frac{\partial^2 u}{\partial t^2} + \frac{8}{9} \gamma |v|^2 u + i \frac{\alpha}{2} u = 0 \\ i \frac{\partial v}{\partial z} - \frac{\beta_2}{2} \frac{\partial^2 v}{\partial t^2} + \frac{8}{9} \gamma |v|^2 v + i \frac{\alpha}{2} v = 0 \end{cases} \quad (1)$$

Here, z and t denote the propagation distance and time coordinates, respectively, whereas α indicate propagation losses. Note that in optical fibers, random spatial fluctuations of the residual birefringence occur in a length-scale of few meters. Averaging out the usual nonlinear Kerr contribution over these fast polarization fluctuations in km-long fibers leads to the so-called Manakov model [22,23]. A corrective factor of 8/9 is then applied to the Kerr

effect due to this polarization randomness and no walk-off term is still present in Eq. (1) between waves u and v [22]. In addition, we assume that third-order dispersion, losses or Raman effects play a minor role in the nonlinear dynamics and can therefore be neglected. Note that the mechanism and analysis should be effective regardless of the value of XPM provided that one could neglect the walk-off between the two waves. This is the case in the present investigation where we have considered sampling and signal waves with wavelengths that are relatively close. Let us also stress that no energy exchange between the u and v waves occurs so that the energy in the sampled signal remains unchanged compared with the unsampled one.

An arbitrary shaped weak signal is first injected into the fiber with a moderate average power (red solid line in Fig. 2(b)). The fiber parameters correspond to the fiber segment used in our experiment and is characterized by a chromatic dispersion $\beta_2 = 3.2 \text{ ps}^2/\text{km}$ and a nonlinear Kerr coefficient $\gamma = 1.7 \text{ W}^{-1}\text{km}^{-1}$. The high power sinusoidal sampling wave (26.5 dBm average power) is then simultaneously injected with an orthogonal polarization state. Note that to ensure an efficient signal processing, the temporal period of this sampling wave has to be much shorter than the signal duration. As already mentioned above in Fig. 1(a), owing to the strong nonlinear defocusing regime, the carrier-suppressed sampling wave is drastically reshaped into the fiber and sharp singularities gradually appear at its null points (see blue line in Fig. 2(a) after 5 km of propagation). Simultaneously, we clearly observe in Fig. 2(b) that the focusing effect imposed by the co-propagating sampling wave progressively leads to a redistribution of the signal energy. Indeed, at the output of the 5-km long fiber, a temporal intensity comb at the sampling rate is then generated upon the signal wave whose amplitude is directly proportional to its initial envelope, thus leading to both a discrete sampling and magnification effect (blue line in Fig. 2(b)). Finally, normalized profiles shown in Fig. 2(c) confirm that the profile of the magnified wave is a perfectly scaled version of the signal under test.

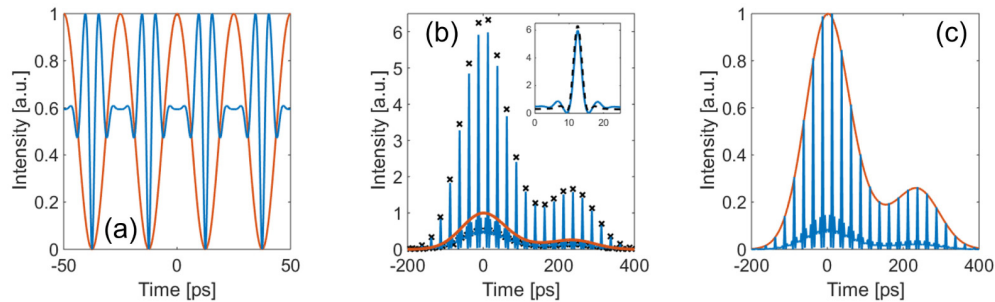


Fig. 2. Numerical simulations (a) Input (red) and output (blue) intensity profiles of the sinusoidal sampling wave normalized to unity for an input average power of 26.5 dBm and 5 km of propagation. (b) Output intensity profiles of the orthogonally polarized signal wave when the pump is deactivated (in red) or activated (blue). The black crosses indicate the maximum values of the theoretical prediction. In the inset, a close view of the numerical and the theoretical estimations. (c) Same as (b) but normalized to unity.

In order to predict the magnification factor experienced upon the sampling process, it proves useful to develop a simplified model based on the analysis of the pump-signal interaction carried out in the optical spectral domain. The cosines-like input $v(0,t) \equiv v(t)_{in}$ pump reads as $v(t)_{in} = (P_0)^{1/2} \cos(\omega_p t)$ to which correspond two spectral components centered at $\pm \omega_p$. The weak input signal is assumed to be a slowly-varying waveform $u(0,t) \equiv u_m(t)$, instead, whose corresponding optical spectrum is centered around $\omega = 0$ with a spectral extension well below ω_p . The FWM interaction among the sampling and signal waves leads to the generation of new spectral components centered around odd (even) multiples of ω_p in

the pump (signal) spectrum. On the other hand, the different power-level of pump and signal makes their longitudinal evolution deeply different. As long as the fiber length does not exceed few nonlinear lengths (defined as $1/\gamma P_0$), the level of the new spectral components generated by FWM in the pump spectrum remains 10 dB below the original components centered at $\pm \omega_p$ [16]. We can thus neglect as a first rough approximation the impact of these additional spectral components and therefore consider that the sinusoidal pump intensity profile is preserved upon propagation except for propagation losses, that is $|v(z, t)|^2 = P_0 \cos(\omega_p t)^2 \exp(-\alpha z)$. Note that this approximation remains still valid as long as the shock point undergone by the sampling wave only occurs in the last stage of propagation, which is the case for most of the power values considered in the present experiment. In contrast, the generation of new spectral components cannot be neglected in the case of the weak signal, instead, as their amplitude rapidly grow up to the peak-level of the input signal spectrum $U(\omega)_{in}$. Replica of $U(\omega)_{in}$ barise in the signal spectrum, centered around even-multiples of ω_p , to which the following ansatz $u(z, t)$ corresponds:

$$u(z, t) = u_{in}(t) \left[\sum S_{2n}(z) \exp(i2n\omega_p t) \right], \quad (2)$$

Insertion of the aforementioned ansatz in Eq. (1) and subsequent collection of terms at the same frequency brings to the following linear system of differential equations (LDE): $\partial S_{2n}(z) / \partial z = (i\alpha_{2n} - \alpha/2) S_{2n} + b(S_{2(n+1)} + S_{2(n-1)})$, being $a_{2n} = 4n^2 \omega_p^2 \beta_2 / 2 + (8/9) \gamma P$. and $b = (4/9) \gamma P$, where $P = P_0 / L \int_{z=0}^L \exp(-\alpha z) dz$ denotes the average pump power along the fiber length. In doing this, we have exploited the slowly-varying hypothesis for $u(t)_{in}$, which allows neglecting all terms in $\partial u_{in} / \partial t$ and $\partial^2 u_{in} / \partial t^2$

Solution of the LDE above requires truncation over a finite number of terms, that is $-N \leq n \leq N$, and the assignment of the input values $S_{2n}(0)$. In practice, $N = 4$ (9 components) is sufficient to get a good estimation of $S_{2n}(z)$. Moreover the input spectrum $U(\omega)_{in}$ is centered around $\omega = 0$, therefore we set $S_0(0)$ and $S_{2n}(0) = 0$ for $n \neq 0$. Note that in the case of a symmetric spectrum, as in the present study, the modeling can be reduced to half of the truncated terms; that is to say only the $n \geq 0$ spectral components can be considered. It is interesting to notice that according to Eq. (2) the input beam $u(t)_{in}$ is modulated by a function Solution of the LDE show that $g(z, t)$ evolves from a constant-in-time function $g(0, t) = 1$ towards a periodic train of pulses that are progressively compressed along the fiber length. Consequently, the signal $u(z, t)$ experiences a simultaneous sampling and magnification, for which samples are more and more temporally compressed and intense upon propagation. In Fig. 1(b), the maxima of the output intensity profile calculated by means of this analytical model have been reported with black crosses and compared to numerical simulations. We can notice a good agreement between both results, thus validating our theoretical approach. Furthermore, in the inset of Fig. 2(b), a close view of both intensity profiles has been depicted and also reveals an excellent prediction of the generated pulse shape. Besides, as we will show in next section, this simplified analytic model well captures the features observed in experiments, and may allow optimizing and engineering the sampling and magnification processes here discussed.

3. Experimental setup and results

The experimental setup depicted in Fig. 3 was implemented in order to provide a proof-of-principle of this technique. For generating both the pump and signal waves, the scheme is initially divided into two arms. In the upper side (sampling beam generation), an external cavity laser emitting at 1550 nm is first intensity modulated thanks to an intensity modulator (IM). A 20-GHz frequency clock is used to drive the IM at its null-transmission point so as to generate a pure carrier-suppressed 40-GHz sinusoidal wave. Note that the fundamental limitation of the present technique is here simply dictated by the electronic bandwidth of the equipments under use. Subsequently, the resulting beating is phase modulated to 100 MHz thanks to a phase modulator (PM) so as to significantly increase the Brillouin threshold above the power levels involved in our experiment [24]. Note that given the significant difference with the sampling frequency, this additional PM does not induce any noticeable consequences on the process under study. On the other side (signal generation), another external cavity laser emitting at the same wavelength is intensity modulated by means of a second IM, which is driven by an arbitrary waveform generator (AWG). Therefore, the profile of this signal consists of a concatenation of two unbalanced Gaussian pulses with a duration of a few nanoseconds. Both the beat-signal (pump) and the arbitrary signal are independently amplified by two Erbium-doped fiber amplifiers (EDFA) and polarization multiplexed thanks to a polarization-beam splitter (PBS). The resulting signals are injected into a 5-km long optical fiber characterized by a chromatic dispersion $D = -2.5$ ps/nm/km at 1550 nm, an attenuation of 0.2 dB/km, a polarization mode dispersion coefficient of 0.05 ps/km^{1/2} (leading to a negligible walk-off between both polarization axes) and a nonlinear Kerr coefficient $\gamma = 1.7$ W⁻¹km⁻¹. Finally, at the output of the system, the resulting sampling and signal waves are polarization demultiplexed thanks to a second PBS and characterized in the time domain by means of two different oscilloscopes (an electrical sampling oscilloscope, ESO with a detection bandwidth of 70 GHz, and an optical sampling oscilloscope OSO from *Alnair Labs* having a temporal resolution of 1 ps). The output signal is also characterized in the spectral domain thanks to an optical spectrum analyzer (OSA).

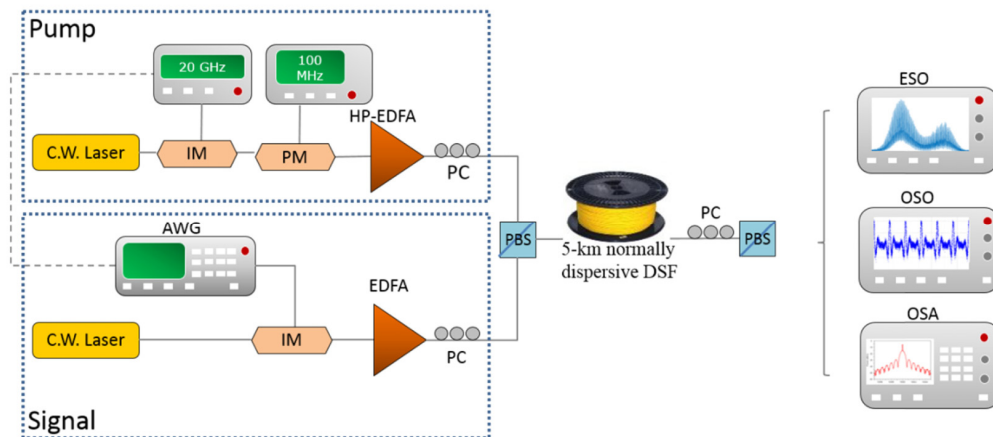


Fig. 3. Experimental setup. IM: intensity modulator, PM: phase modulator, AWG: arbitrary waveform generator, EDFA: Erbium-doped fiber amplifier, PC: polarization controller, PBS: polarization beam splitter, ESO: electrical sampling oscilloscope, OSO: optical sampling oscilloscope and OSA: optical spectrum analyzer.

The power of the incident signal is kept constant to 10 dBm while the pump power varied from 16 to 28 dBm. Figure 4(a) displays the normalized envelope of the arbitrary shaped nanosecond signal monitored at the output of the fiber when the sinusoidal pump wave is off (in red) and after the sampling process for an injected pump power of 26.5 dBm (in blue). We

clearly observe a high-repetition-rate pulse train distributed along the signal wave and generated at the modulation frequency of the pump whose amplitude perfectly matches the initial signal envelope. We can thus notice that the sampling process acts in full strength whilst the shape of the signal is well preserved, in good agreement with our numerical predictions of Fig. 2(c). It is noteworthy that for the results displayed in Fig. 4(a), both signal and sampling waves were synthesized thanks to the same initial RF clock and consequently appear temporally synchronized, which allows us to efficiently monitor the generation of the pulse train along the signal profile. Simultaneously, the sinusoidal pump wave has been broadened due to the combined effects of SPM and chromatic dispersion and undergoes an optical shock as illustrated in Fig. 4(b) for an injected power of 26.5 dBm, in full agreement with the trend reported in Figs. 1(a) and 2(a).

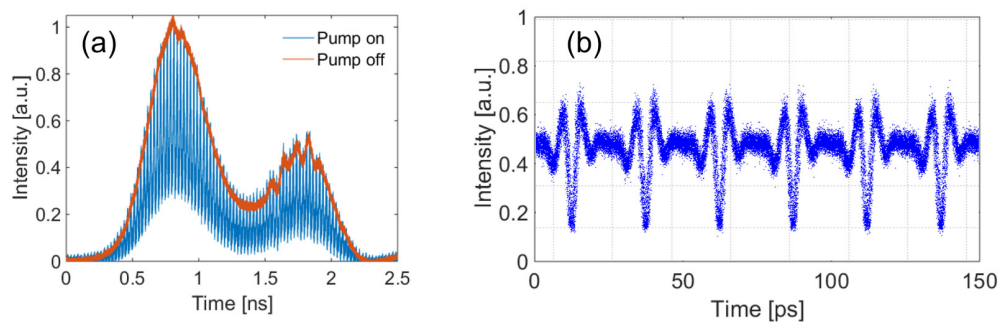


Fig. 4. (a) Normalized output signal in the temporal domain. For the red line, the pump is off and, for the blue curve, the signal is sampled (pump power equal to 26.5 dBm). This figure is obtained with the ESO. (b) Output intensity profile of the pump beam (power equal to 26.5 dBm). This snapshot is obtained with the OSO.

As it was previously mentioned, apart from the sampling process, the intensity profile of the signal wave is simultaneously magnified. The magnifying factor of the signal shape recorded at the output of the fiber as a function of the injected pump power has been reported in Fig. 5. Here, signal and sampling waves are not temporally synchronized anymore (i.e. the sampling frequency is not an integer number times the repetition rate of the signal to be analyzed). Therefore, the pulse train generated along the signal wave cannot be efficiently resolved anymore. Consequently, by acquiring multiple traces of the signal wave and superposing them, we get a cloud of points for which the full envelope leads to the resulting magnified signal reconstruction. Figure 5(a) compares the intensity profiles of a 1.5-ns arbitrary signal recorded at the output of the fiber with and without the presence of the 40-GHz sinusoidal sampling wave, for different injected powers. We can notice that the output signal can reach a magnification factor close to 7 (8.5 dB) when the sampling wave is activated. In particular, it is noteworthy that the second Gaussian pulse superimposed on the trailing edge of the arbitrary signal was hardly observable when the sampling beam is off, whereas it can be easily detected when the signal is intensity magnified. In Fig. 5(b), we have reported the experimental magnifying factor (blue circles) of the output nanosecond signal as a function of the injected power of the sampling wave. First of all, we can notice that the factor of magnification is not perfectly proportional to the sampling wave and that a maximum gain of 8.5 dB can be achieved owing to the present configuration. Experimentally, the power of the sampling beam is here limited to 28 dBm because of the Brillouin backscattering effect. Therefore, we have optimized the length of the fiber under use so that the normal dispersion regime can optimally compensate for the cross-phase modulation induced by a 28-dBm sampling beam. These experimental results have been compared both to numerical simulations (red solid line) and to our theoretical predictions (black crosses) assuming the simplified model described in the above section. We can observe an excellent

agreement between our experimental measurements and both numerical as well as theoretical estimations, thus validating the present technique and its Manakov modeling.

Finally, the output signal is analyzed in the spectral domain. The phenomenon can be characterized as the generation of new spectral components at the pump frequency (40 GHz) related to the time-dependence of the nonlinear phase shift induced by XPM as illustrated in Fig. 5(c). The experimentally recorded spectrum exhibits an optical signal to noise ratio higher than 40 dB, which confirms that our magnification process does not suffer from unwanted amplified spontaneous emission noise. Moreover, we can observe once again a good agreement between the output recording spectrum and our theoretical predictions. Note that the disagreement among theoretical and numerical/experimental spectra grows larger as the pump power increases. This discrepancy at large pump power is related to the generation of new spectral components in the pump spectrum through FWM which, combined to chromatic dispersion, leads to severe distortion of its intensity profile; effect neglected in our present theoretical approach. Nevertheless, these components mainly affects the phase profile of the generated pulse signal, while not the magnitude. For this reason a good agreement between theoretical and numerical/experimental intensity profiles is still achieved for large pump powers (see Fig. 2(b)).

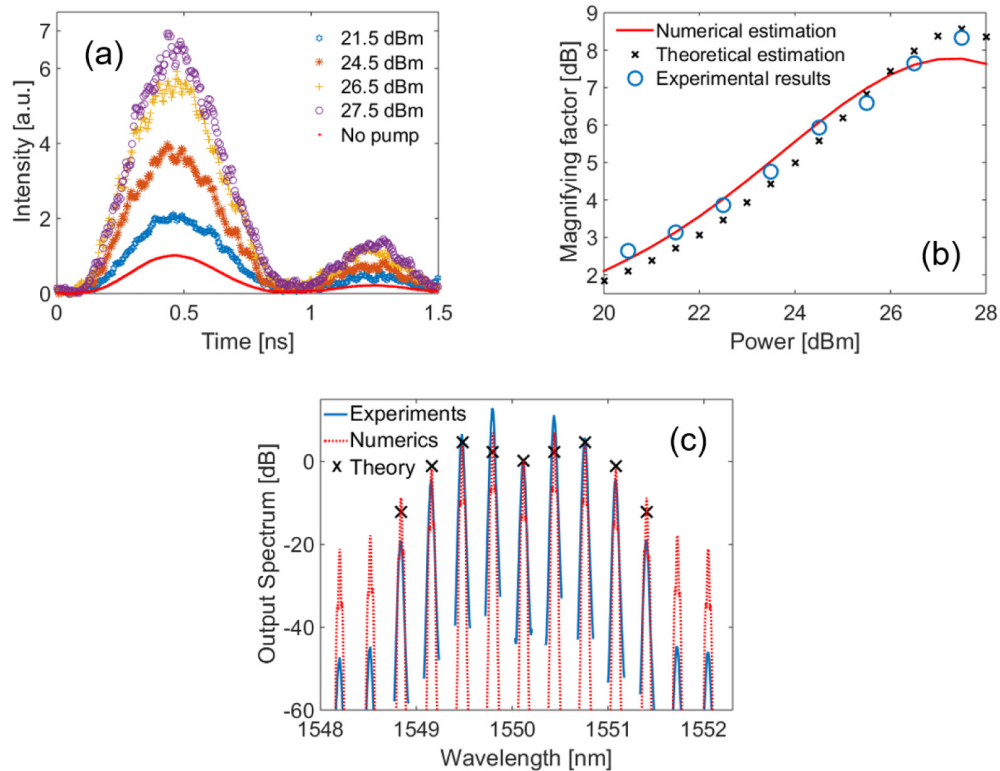


Fig. 5. (a) Output signal in the temporal domain. For the red line, the pump is off and the signal is magnified for different injected powers. This figure is obtained with the OSO and only the envelope is drawn. (b) Magnifying factor of the output signal as a function of the injected pump power. The experimental values (blue circles) are compared with the numerical simulations (red line) and theoretical predictions (black crosses). (c) Experimental spectra of the output signal (in blue) compared to theoretical (black crosses) and numerical estimations (red dashed line) for a pump power of 26.5 dBm.

4. Conclusions

In summary, we have proposed and experimentally demonstrated a novel technique enabling to simultaneously sample and magnify an arbitrary shaped optical signal. The present system is based on a periodic focusing effect upon an incident signal which takes place in a normally dispersive medium by means of a cross-phase modulation interaction induced by an orthogonally polarized high-repetition-rate sinusoidal pump wave. This localized periodic focusing induces a redistribution of energy along the signal profile which leads to the generation of a temporal comb at the repetition frequency of the pump whose amplitude is directly proportional to the incident signal, thus enabling its sampling and magnification. No amplification spontaneous emission noise is observed in the magnification process that does not involve any active gain medium. Using this technique, we have successfully implemented a 40-GHz sampling operation as well as an 8-dB magnification of an arbitrary shaped nanosecond signal around 1550 nm within a 5-km long normally dispersive optical fiber. Numerical and theoretical results are in good agreement with our experimental recordings. Alternatives based on wavelength multiplexed waves instead of polarization multiplexed waves could be developed, but the walk-off between the pump and signal may ultimately in such configuration degrade the efficiency of the magnification due to the focusing effect.

Funding

This research is funded by the European Research Council under Grant Agreement 306633, ERC PETAL (www.facebook.com/petal.inside).